AGU PUBLICATIONS

Geophysical Research Letters

RESEARCH LETTER
10.1002/2016GL069973

Key Points:
- Storm-elevated subsurface vertical diffusion accesses the subsurface iron reservoir
- Intraseasonal entrainment of subsurface iron sustains primary production through summer
- This requires a transition layer of strong diffusivities beneath the surface mixed layer

Supporting Information:
- Supporting Information S1
- Figure S1

Correspondence to:
S.-A. Nicholson,
sarahanne.n@gmail.com

Citation:
Nicholson, S.-A., M. Lévy, J. Llort, S. Swart, and P. M. S. Monteiro (2016), Investigation into the impact of storms on sustaining summer primary productivity in the Sub-Antarctic Ocean, *Geophys. Res. Lett.*, *43*, 9192–9199, doi:10.1002/2016GL069973.

Received 14 JUN 2016
Accepted 25 AUG 2016
Accepted article online 28 AUG 2016
Published online 14 SEP 2016

Investigation into the impact of storms on sustaining summer primary productivity in the Sub-Antarctic Ocean

Sarah-Anne Nicholson[1,2,3], Marina Lévy[1], Joan Llort[1], Sebastiaan Swart[2,3], and Pedro M. S. Monteiro[2,3]

[1]Sorbonne Universités (UPMC, Paris 6)/CNRS/UPMC/IRD/MNHN, Laboratoire d'Océanographie et du Climat (LOCEAN), Institut Pierre Simon Laplace (IPSL), Paris, France, [2]Southern Ocean Carbon-Climate Observatory, CSIR-CHPC, Cape Town 7700, South Africa, [3]Department of Oceanography, University of Cape Town, Rondebosch, South Africa

Abstract In the Sub-Antarctic Ocean elevated phytoplankton biomass persists through summer at a time when productivity is expected to be low due to iron limitation. Biological iron recycling has been shown to support summer biomass. In addition, we investigate an iron supply mechanism previously unaccounted for in iron budget studies. Using a 1-D biogeochemical model, we show how storm-driven mixing provides relief from phytoplankton iron limitation through the entrainment of iron beneath the productive layer. This effect is significant when a mixing transition layer of strong diffusivities ($k_z > 10^{-4}\,m^2\,s^{-1}$) is present beneath the surface-mixing layer. Such subsurface mixing has been shown to arise from interactions between turbulent ocean dynamics and storm-driven inertial motions. The addition of intraseasonal mixing yielded increases of up to 60% in summer primary production. These results stress the need to acquire observations of subsurface mixing and to develop the appropriate parameterizations of such phenomena for ocean-biogeochemical models.

1. Introduction

An unexplained peculiarity of phytoplankton blooms in the Southern Ocean (SO) is the regional-scale occurrence of prolonged blooms into late summer [*Swart et al*., 2015; *Carranza and Gille*, 2015]. Observations of chlorophyll *a* show that summer blooms are widespread and occur annually [*Carranza and Gille*, 2015], are prominent within the Sub-Antarctic Zone (SAZ), and may be several months in duration (e.g., ~16 weeks in *Racault et al*. [2012]), typically initiating in spring (~September–November) [*Thomalla et al*., 2011] and terminating in late summer [*Swart et al*., 2015]. These regions of high chlorophyll are mostly associated with high primary production (PP) [*Arrigo et al*., 2008] and are particularly puzzling as they occur at a time when strong iron limitations should prevent growth [*Boyd*, 2002], yet summer productivity has been noted in a number of studies [*Park et al*., 2010; *Thomalla et al*., 2011; *Frants et al*., 2013; *Carranza and Gille*, 2015; *Swart et al*., 2015].

A possible explanation for the presence of late summer productivity is the biological recycling of iron within the summer surface mixed layer [*Tagliabue et al*., 2014]. This hypothesis is supported by iron budget-based studies [*Boyd et al*., 2005; *Bowie et al*., 2009] and is consistent with observations of low *fe ratios* during summer (i.e., the proportion of dissolved iron (DFe) uptake from "new" sources [*Boyd et al*., 2005]). In this seasonal scenario, after a "once-off" winter entrainment flux of DFe (estimated to be 9.5–33.2 $\mu mol\,DFe\,m^{-2}\,yr^{-1}$), surface DFe is depleted rapidly by the proliferation of phytoplankton in spring. In summer, estimates of physical supplies of diapycnal diffusion (~2 $\mu mol\,DFe\,m^{-2}\,yr^{-1}$) and Ekman upwelling (−0.7 $\mu mol\,DFe\,m^{-2}\,yr^{-1}$) are too low to meet the observed utilization rates of phytoplankton, and the biological recycling of iron of ~5–10 $\mu mol\,m^{-2}\,d^{-1}$ is required to close the summer budget.

This study examines the possibility of an additional storm-driven physical supply of DFe, which may complement biological recycling: we explore whether storms, which occur at periods 4–10 days [*Swart et al*., 2015] with life spans of 1–12 days [*Yuan et al*., 2009], may contribute to this summer budget. Midlatitude storms occupy vast extents of the SO (e.g., radii of up to ~1000 km [*Yuan et al*., 2009]), are prominent in austral summer [*Swart et al*., 2015; *Carranza and Gille*, 2015], occur in regular succession (e.g., *Yuan et al*. [2009] observed 271 storms in the summer of 2001), and inflict strong open ocean winds (e.g., speeds $> 20\,m\,s^{-1}$ [*Yuan*, 2004]). Increasing evidence suggests that these transient wind events drive strong intraseasonal variability in chlorophyll that can dominate the seasonal variability [*Thomalla et al*., 2011]. Intraseasonal enhancements in summer chlorophyll have been linked to perturbations in the extent of the mixed-layer depth (MLD)

[*Fauchereau et al*., 2011], which matched the storm-driven wind stress variability [*Carranza and Gille*, 2015; *Swart et al*., 2015]. These studies have hypothesized that the regular storm-driven vertical entrainment of iron could sustain the bloom into late summer.

Summer storms induce energetic "instantaneous" vertical mixing events, where upper ocean k_z are of the order of $10^{-1}\,m^2\,s^{-1}$ [*Cisewski et al*., 2005; *Forryan et al*., 2015]. This energy contributes to the formation and deepening of the surface-mixing layer [*Price et al*., 1978]. We refer to this strongly turbulent "surface-mixing layer" as the *SXLD*. Wind-driven energy has also been shown to excite strong inertial motions within the upper ocean, which may last several days to weeks poststorm (e.g., present 23 days poststorm in *D'Asaro et al*. [1993]) and result in enhanced shear-driven vertical mixing below the base of the SXLD within a "mixing transition" layer [*Polton et al*., 2008; *Dohan and Davis*, 2011; *Forryan et al*., 2015]. The vertical extent of this transitional subsurface mixing layer is referred to here as the "*XLD*". In the presence of mesoscale and submesoscale ocean variability this wind-driven inertial energy is concentrated [*Klein and Lapeyre*, 2004; *Zhai et al*., 2005; *Lévy et al*., 2009; *Jing et al*., 2011; *Meyer et al*., 2015] and may further impact the extent and magnitude of mixing in the XLD. These small-scale features may enhance the downward propagation of inertial energy into the subsurface ocean [*Lee and Niiler*, 1998; *Zhai et al*., 2005; *Jing et al*., 2011] and potentially induce the rapid breaking of near-inertial waves to produce intense vertical mixing [*Meyer et al*., 2015]. Thus, storm-eddy interactions are believed to be important in the furnishing and enhancing of subsurface vertical mixing [*Zhai et al*., 2005; *Jing et al*., 2011; *Meyer et al*., 2015; *Forryan et al*., 2015]. It is expected that this mechanism could be important in the SO, a region of high eddy kinetic energy [*Daniault and Ménard*, 1985] and strong inertial momentum from passing storms [*Wang and Huang*, 2004]. However, direct observations of these interactions are sparse; thus, it remains uncertain how this storm-driven mixing energy will alter the magnitude and shape of the mean upper ocean vertical diffusion profiles particularly in a dynamically complex ocean.

In this study we follow a sensitivity analysis approach with a 1-D biogeochemical model and two idealized cases of upper ocean mixing by storms: the role of only a deepening of the surface-mixing layer during the storm and the role of an additional enhancement of poststorm subsurface mixing. We assess if the supply of new iron to the surface waters by such two mixing scenarios is sufficient to match phytoplankton growth requirements during summer to sustain the bloom.

2. Model and Experimental Design

We used the 1-D biogeochemical model PISCES [*Aumont and Bopp*, 2006] setup to represent the mean seasonal evolution of PP in the open ocean domain of the SAZ [*Llort et al*., 2015]. We perturbed the model with intraseasonal mixing events during summer. The biogeochemical model was forced with surface photosynthetic available radiation (PAR), vertical mixing, and temperature, which were analytically prescribed "offline"; i.e., there is no physical model. The seasonal and intraseasonal vertical mixing were prescribed using idealized vertical mixing coefficient (k_z) profiles. Prescribing the k_z profile allowed for full control on the strength of the summer perturbations instead of relying on vertical mixing parameterizations, an important aspect as there remain uncertainties in the way the impact of strong storms is parameterized.

The depth of the surface-mixing layer changed throughout the year. More precisely, three main seasonal mixing phases have been represented: a deepening SXLD during winter convection, a shoaling SXLD during the suspension of convection in spring, and a constantly shallow SXLD due to strong buoyancy forcing in summer. The timing and depth of these seasonal mixing characteristics, namely, the winter maximum (MLD_{max}: 250 m, 350 m, and 450 m) and summer minimum (MLD_{min}: 30 m, 50 m, and 70 m) were changed iteratively, allowing for an ensemble (53 seasonal cycles) of different SAZ conditions to be explored (Figure 2a). As a first guess, we assumed that the density-based MLD is a good approximation of the SXLD, and thus, these characteristics were constructed according to Argo MLD observations [*Hosoda et al*., 2011]. Such seasonal iterations represent the "control" runs, which exclude intraseasonal mixing events.

To represent the impact of intraseasonal wind events on the summer SXLD, these seasonal mixing cycles were modified to include transient deepening of the SXLD with fixed amplitudes of +45 m and periods of 7 days with 5 days between each deepening event, referred to as the "*SXLD deepening*" runs. These values represent the mean characteristics of temperature-based MLD perturbations estimated from glider data [*Swart et al*., 2015]. The number of perturbations in summer also varied between 4 and 6 events depending

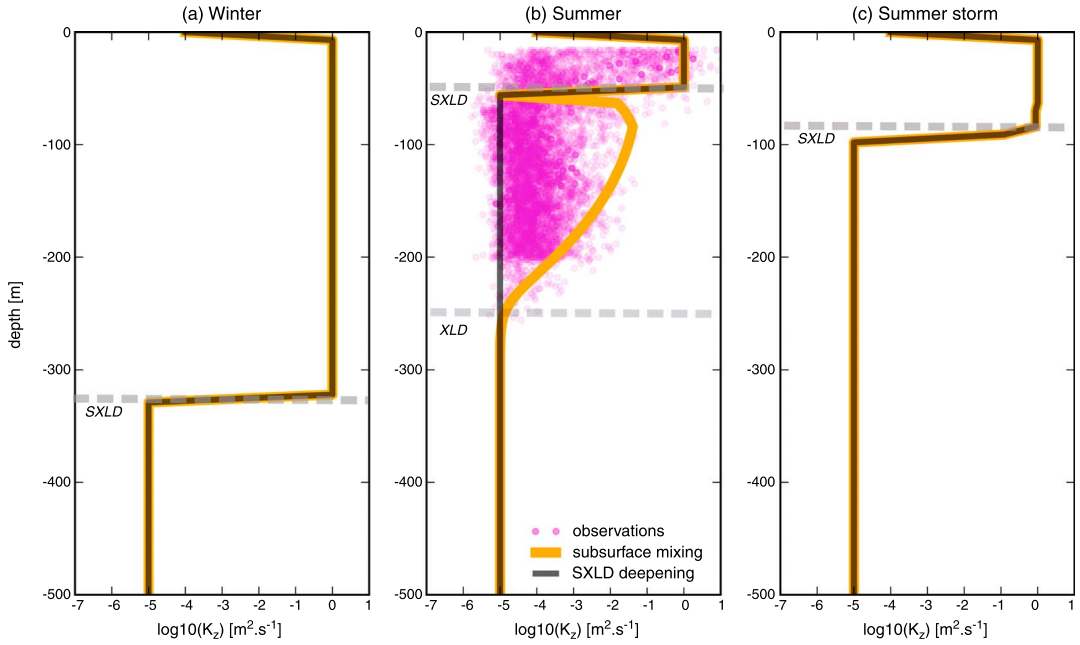

Figure 1. The prescribed k_z ($m^2\,s^{-1}$) profiles of (a) winter, (b) summer (poststorm), and (c) during a summer storm. Two idealized cases: SXLD deepening (black) with slow mixing beneath the strong surface mixing and subsurface mixing with an enhanced gradient of mixing beneath the SXLD after summer storms (orange) and constrained summer k_z observations (magenta) in the ACC [*Forryan et al*., 2015].

on the start of the summer minimum (15 November or 15 December) until 15 February. This was consistent with the number of events from the 7 day Empirical Mode Decomposition of the MLD data observed in *Swart et al*. [2015]. In the SXLD deepening runs (Figure 1), we prescribed small constant open ocean mixing ($k_z = 1e^{-5}\,m^2\,s^{-1}$) directly beneath a thoroughly "mixing" surface layer SXLD ($k_z = 1\,m^2\,s^{-1}$, such that phytoplankton were evenly distributed vertically within this layer [*Lévy*, 2015]).

However, as discussed, turbulent mixing can extend well below what can be explained by the SXLD. In a second set of experiments—the "*subsurface mixing*" runs—we explored the impact of the interior mixing due to inertial motion set by passing storms. Inertial-driven subsurface mixing may persist for several days to weeks after the storm, after the deepened SXLD has restabilized to the surface. Typically observed in vertical profiles of stratification and density is a sharp density step at the base of the mixed layer where a stratification maxima is found, below which a gradient of decreasing but high stratification and vertical shear occur [*Johnston and Rudnick*, 2009]. At the point of maximum stratification we set k_z to a minimum value ($k_z = 1e^{-5}\,m^2\,s^{-1}$) as observed by *Cisewski et al*. [2005] and *Sun et al*. [2013], directly beneath this minimum, we enhanced the subsurface k_z for several days after each storm event. By setting k_z to a minimum directly beneath the SXLD, we were able to ensure that the enhanced subsurface mixing would not result in a deeper SXLD, as shown in an additional passive tracer experiment (Figure S1 in the supporting information). In these subsurface mixing runs, we alternate between phases of SXLD deepening and subsurface mixing for the duration of summer. The magnitude of the subsurface mixing is constrained to k_z data collected during summer in a frontal region of the Antarctic Circumpolar Current (ACC) by *Forryan et al*. [2015].

In all runs, for the prescription of temperature and surface PAR, we used an averaged (40–60°S) climatological seasonal cycle (DFS3-ERA40 [*Brodeau et al*., 2010]). The initial vertical profile for dissolved iron was constructed according to mean observational ranges [*Tagliabue et al*., 2012] and set to 0.15 nmol L^{-1} above a ferricline depth of 333 m [*Tagliabue et al*., 2014] with 0.5 nmol L^{-1} below. Given the range of prescribed winter SXLD maximums (which may reset the depth of the ferricline if $>$ 333 m), after the first year of simulation our resulting range of explored summer ferriclines varied between ~333 m and ~450 m. The initial profiles for macronutrients (nitrate, phosphate, and silicate) were based on winter mean profiles from KERFIX [*Jeandel et al*., 1998]. The model parameters were unchanged from the global setup of PISCES-V1 [*Aumont and Bopp*, 2006]. With this set of parameters, iron remineralization is not sufficient to sustain the summer bloom

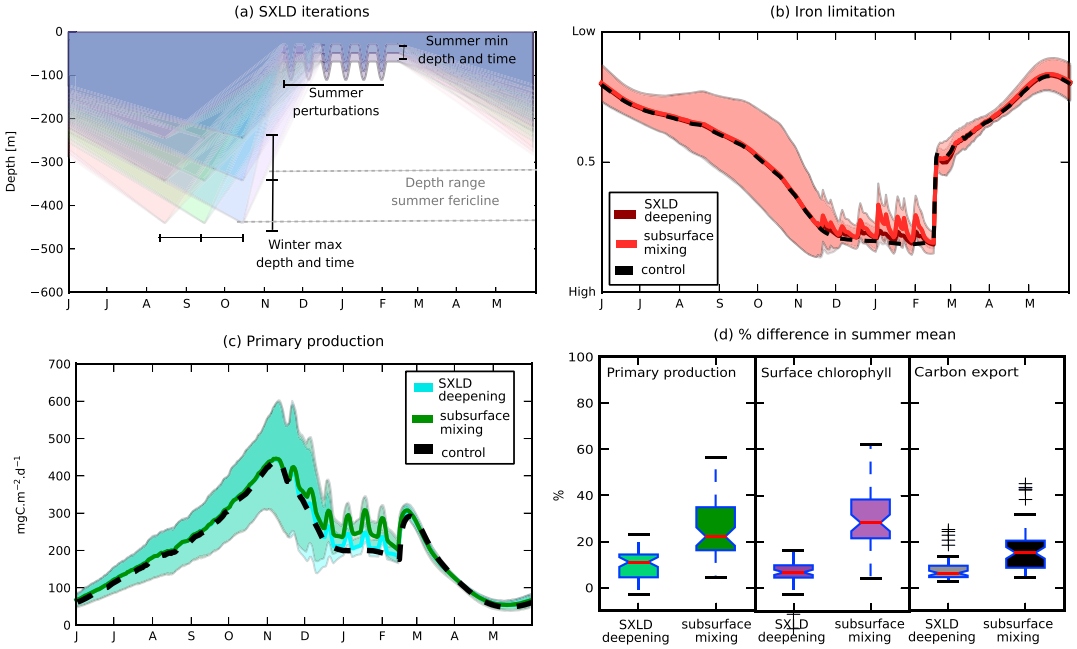

Figure 2. (a) Seasonal iterations of SXLD (m), (b) simulated iron limitations on phytoplankton, (c) integrated PP (mg C m^{-2} d^{-1}), and (d) the percentage mean change in summer PP, surface chlorophyll, and carbon exported at 250 m (i.e., [subsurface mixing runs − control runs]/control runs). Shading = standard deviation; solid line = mean of all iterations. Black dashed line = mean of control runs.

in the control runs. The simulations were integrated for 3 years to allow for the biological terms to reach a repeating seasonal cycle. The results are based on the third year of integration.

3. Model Results

3.1. Control Runs

The seasonal range of PP in our control runs falls within the estimates of *Arrigo et al.* [2008] (~50–450 mg C m^{-2} d^{-1}) for open ocean waters in the SO (black dashed line, Figure 2c). The peak of productivity occurs during spring (approximately September to November) but rapidly declines at the start of the summer (approximately December). During this period, the seasonal iron limitations of phytoplankton are the strongest and persist as so through summer resulting in low productivity (Figure 2b). In a summary of the total summer iron stocks and fluxes for the summer MLD_{min} (following the approach of *Bowie et al.* [2009, 2015]) the physical supply of DFe (13 ± 11 nmol DFe m^{-2} d^{-1} via vertical diffusion only) is minor (Figure 3a). Despite the remineralization supply (comprising disaggregation of small particulate iron, SFe = 320 ± 27 nmol DFe m^{-2} d^{-1}, and zooplankton, Zoo = 720 ± 51 nmol DFe m^{-2} d^{-1}) being higher, it is unable to meet the phytoplankton demand and thus sustain high summer productivity. After the summer phase, when the SXLD deepens, a secondary peak of PP (an "autumn bloom") developed in response to this deepening.

3.2. SXLD Deepening Runs

In our SXLD deepening runs, we perturbed the SXLD of the control runs with intraseasonal deepening events in summer. The seasonal evolution of our simulated mean PP (Figure 2c) remained almost identical to the control runs apart from summer. During summer, a small increase in PP was associated with each SXLD mixing event, corresponding to minor decreases in iron limitation. The summer remineralization supply remained unchanged from the control run; thus, the small increase in productivity at each perturbation highlights the additional supply of new iron from vertical diffusion (54 ± 40 nmol DFe m^{-2} d^{-1}) and entrainment (198 ± 44 nmol DFe m^{-2} d^{-1}) (Figure 3b). The standard deviation of PP (shading in Figure 2c), which reflects the varied response to different seasonal mixing cycles, is less in summer than in spring, indicating that the response of summer PP to summer SXLD deepening events is robust over a range of seasonal cycles.

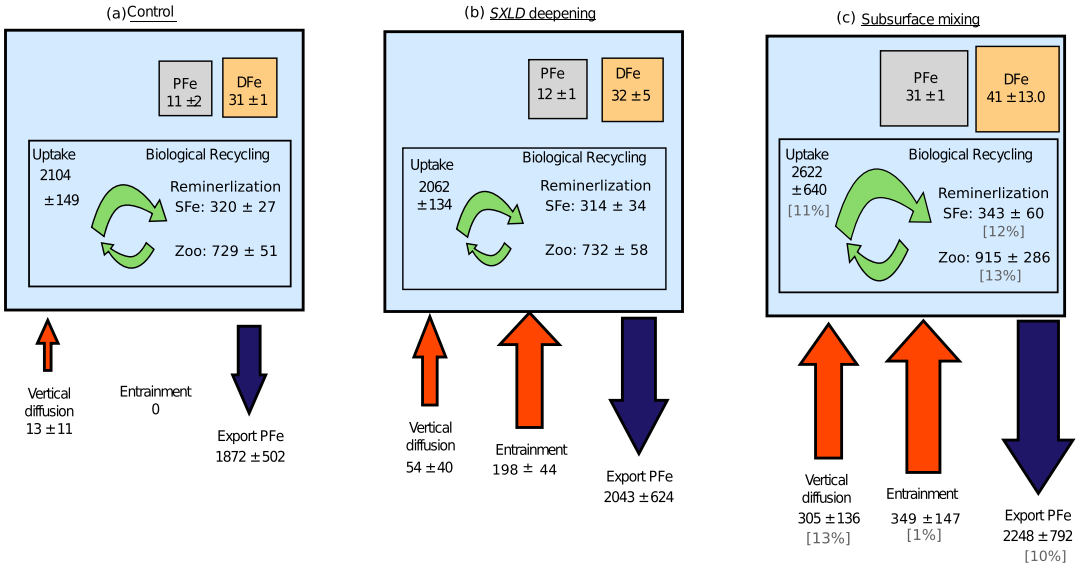

Figure 3. Summer standing stocks (μmol m^{-2}) and fluxes (nmol m^{-2} d^{-1}) of iron for the upper MLD_{min}: (a) *Control*, (b) SXLD deepening, and (c) subsurface mixing runs following the approach of *Bowie et al.* [2015]. The export of PFe is computed at 250 m. Remineralization includes disaggregation of small particulate iron (SFe) and zooplankton excretion and sloppy feeding (Zoo). The percentage that each summer value represents over the total annual mean is also provided (gray text).

3.3. Subsurface Mixing Runs

The addition of subsurface mixing after the SXLD deepening events in summer resulted in a further reduction in the strength of phytoplankton iron limitation (Figure 2b), and as a consequence, at each mixing event, there was an enhancement in the mean PP on the order of 100–140 mg C m^{-2} d^{-1}. Intraseasonal increases of similar magnitude were found by *Thomalla et al.* [2015]. Although mixing to depth also increased phytoplankton light limitation, the reduction in light exposure was not enough to alter growth. In this ensemble, in relation to the SXLD deepening runs the total vertical iron supply (654 ± 283 nmol DFe m^{-2} d^{-1}) increased by 56%. Additionally, the remineralized supplies of iron increased (SFe by 7% and Zoo by 20%). This was due to increases in biogenic particulate iron (in PISCES particulate iron is remineralized in proportion to the particulate iron pool) and increases in zooplankton biomass. Our simulated summer ranges of vertical DFe supply fall within observed values of 94–1112 nmol DFe m^{-2} d^{-1} [*Bowie et al.*, 2015], and the remineralized supply agrees with ranges in *Bowie et al.* [2009] of 261–1206 nmol DFe m^{-2} d^{-1}. Importantly, a comparison with the total iron budget (Table S1) shows that the summer period accounts for a small percentage of the total iron supply and uptake (Figure 3c). Despite the summer vertical iron supplies being considerably smaller than the winter entrainment flux estimated to be ~42 ± 19 μmol DFe m^{-2} yr^{-1}, similarly shown in *Tagliabue et al.* [2014], these results suggest that the contribution of storm-driven mixing may play a role in providing some relief from strong Fe limitation during summer through impacts on the efficiency of both the "new" and "regenerated" fluxes of DFe.

3.4. Response of Summer PP and Surface Chlorophyll to Intraseasonal Mixing

The response of PP and surface chlorophyll in summer can be quantified in terms of the percentage mean change (i.e., [subsurface mixing runs − control runs]/control runs). We exclude the spring and fall bloom from the summer mean. The lower range of percentage increases in the summer mean PP and surface chlorophyll (Figure 2d) are associated with the SXLD deepening ensemble (~−3–22%), which prescribes no impact of storm-driven mixing beneath SXLD, while the upper ranges (~10–60%) are associated with the subsurface mixing ensemble with a strong effect of the storm-driven mixing beneath the SXLD (Figure 2d). The spread of the percentage mean change reflects the sensitivity of the response to the number of perturbations, the depth of the winter mixing, the summer ferricline, and the summer mixing, i.e., to the range of environmental conditions in the SAZ.

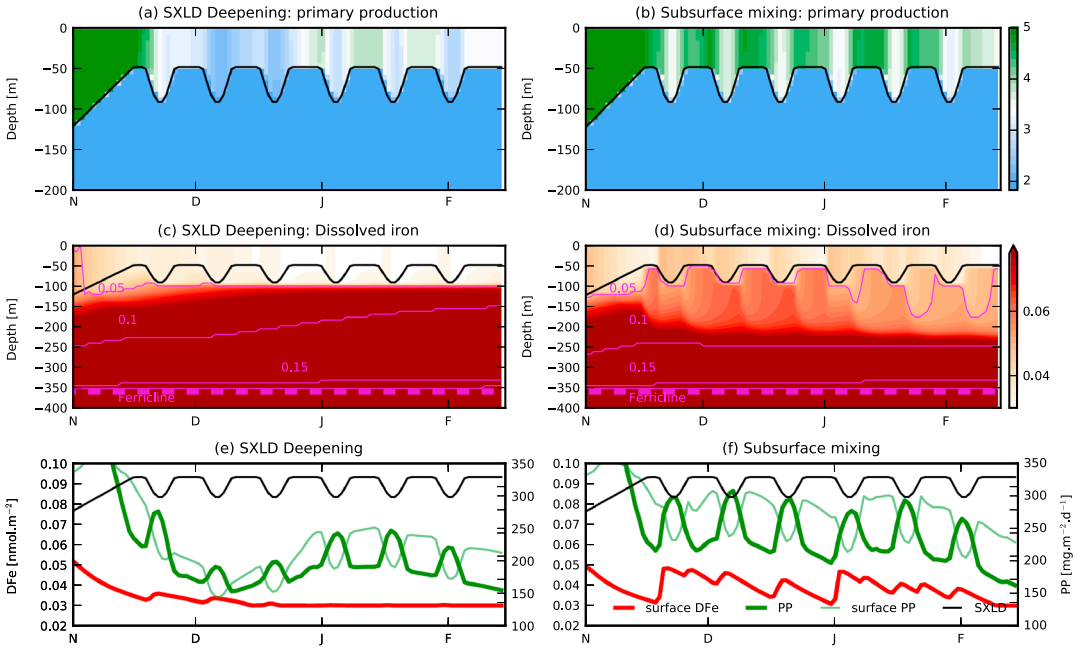

Figure 4. Comparisons of (a and b) primary production (mg C m^{-3} d^{-1}), (c and d) DFe (nmol L^{-1}), and (e and f) integrated PP, surface PP*64, SXLD, and surface DFe between the SXLD deepening and subsurface mixing run.

In addition, we compute the particulate carbon export at a depth beneath any active mixing (e.g., 250 m). The subsurface mixing runs with the strongest "storm impact" on vertical mixing and the largest increases in summer PP had the highest increase in carbon export flux (between 12 and 45%). The spring bloom had carbon export values which ranged between ~3 and 14.8 mmol C m^{-2} d^{-1}, and the sustained bloom production in summer between ~3 and 8 mmol C m^{-2} d^{-1}. With the assumption that remineralization was low above the base of our XLD, our export falls within the range of particulate organic carbon export observed by *Morris and Charette* [2013] of ~ 5–15 mmol C m^{-2} d^{-1} at 100 m during CROZEX from November to December.

4. Discussion

Using a 1-D biogeochemical model with two idealized storm-driven vertical mixing scenarios, we illustrated how strong transient vertical mixing events beneath the surface mixing layer may help sustain summer production. We now discuss this response by comparing the results from our control runs (no summer storms) and our two ensembles with summer storms.

In the control runs, DFe was supplied into the surface layers by a once-off deepening of the SXLD in winter with no entrainment terms in summer. During spring, DFe was consumed rapidly (when the SXLD shoals, Figure 2b). In summer, mixing at one constant depth meant that the only physical supply of DFe available for consumption was via the slow diffusive flux across the SXLD boundary. Our control runs were unable to simulate observed sustained PP.

To summarize the response of the storm-driven vertical mixing scenarios, a seasonal iteration of the upper ocean summer DFe and PP is compared (Figure 4). In our SXLD deepening runs, despite the addition of intraseasonal SXLD perturbations, PP (Figure 4a) declined shortly after the spring bloom as in the control runs. The DFe was depleted (<0.05 nmol L^{-1}) in the upper layer corresponding to first SXLD summer perturbation (~100 m) by the vertically homogenous proliferation of phytoplankton setting an upper ocean gradient of DFe at this depth. The prescribed weak vertical diffusion beneath the SXLD was unable to further diffuse the deeper DFe reservoir rapidly enough for it to be entrained by the next SXLD perturbations. The synoptic mixing events were unable to entrain a sufficient supply of DFe (Figures 4c and 4e) to meet the iron demands of PP.

In contrast, in the subsurface mixing case, the enhanced subsurface mixing (for 5 days) after each SXLD deepening event allowed the iron just below the SXLD to be refurnished, and thus, the next SXLD perturbations could entrain this DFe to the surface (Figures 4b and 4f). The refurbishment of the subsurface DFe reservoir

also meant that the gradient between the subsurface and surface DFe was enhanced resulting in increased diffusive fluxes of DFe across the SXLD (Figure 3c). The integrated PP responded rapidly to this intraseasonal supply of DFe, increasing when the SXLD deepened with a maximum integrated PP occurring during the time of maximum SXLD (Figure 4f). The minimum surface PP values occurred during the maximum SXLD, when phytoplankton were diluted to deeper depths, resulting in a temporal phase lag (~5 days) between the maximum peaks of surface and integrated PP.

Thus, such short-term synoptic mixing events (storms), whose energy into the interior of the ocean may be underestimated, could be making an important contribution in accessing the subsurface DFe reservoir. SXLD deepening events occurring in regular succession could not substantially raise summer productivity and chlorophyll; however, coupled with enhancements in subsurface k_z, they act as an effective mechanism to increase production throughout summer. We propose that the link between storms and new DFe supply is through these alternating dynamical responses of the water column physics. Such physical drivers not only enhanced the new sources of DFe increasing PP but also have positive feedbacks on the remineralized supply, which together sustained summer PP.

We have tested our hypothesis under a wide range of plausible SAZ environmental conditions. As seen by the spread in the percentage mean change in Figure 2d, there are cases when such prescribed mixing does not result in a large response in summer PP and surface chlorophyll (e.g., seasonal cycles with shallow winter SXLD's, fewer storm events, and shallow summer SXLD). Therefore, the success of our storm mixing profiles to sustain a bloom is also dependent on the seasonal characteristics of the SXLD and the ferricline depth, which may help to explain the regional occurrence of such blooms. A number of idealizations have been made in the construction of the 1-D model; thus, these results should be interpreted with care. Our experiments have been designed so that the only limiting nutrient is dissolved iron; thus, regions in the SAZ where silicic acid limitations dominate [*Boyd*, 2002] are not represented here.

5. Conclusion

We used a 1-D model sensitivity analysis approach to explore the mechanistic basis for an additional source of iron in summer that could explain how phytoplankton blooms in the SAZ can be sustained through summer. Our results suggest that intraseasonal mixed-layer perturbations, linked to storms, may offer relief from Fe limitation in summer, particularly if there is sufficient k_z subsurface mixing ($k_z \sim O(10^{-4}–10^{-1})\ m^2\ s^{-1}$) beneath the surface mixing layer. This process may work in unison with other mechanisms that may additionally contribute to the replenishment of iron, such as remineralization, lateral advection, or vertical pumping associated with mesoscale and submesoscale processes and should be accounted for in future iron budgets. The vertical mixing values needed to sustain this additional summer productivity were considerably higher than mean estimates ($k_z \sim O(10^{-5}–10^{-4})\ m^2\ s^{-1}$) but within reach of the upper bounds of individually observed profiles beneath the mixed layer [*Cisewski et al*., 2005, 2008; *Forryan et al*., 2015]. The impact of such mixing events was in increasing summer PP by up to 60%. This was shown to have implications for carbon export, resulting in higher summer export fluxes. Understanding the sensitivity of summer productivity in the SO to storm-driven upper ocean mixing may help to better understand the sensitivities of the carbon cycle to both short-term variability and long-term trends in large-scale atmospheric forcing.

Acknowledgments
The authors thank Alexander Forryan for the k_z data available on request from http://www.bodc.ac.uk. This work was supported by CSIR Parliamentary Grant, the NRF-SANAP grant SNA14071475720, and the research staff exchange SOCCLI program (FP7-PEOPLE-2012-IRSES). S. Swart acknowledges the support of a CSIR-YREF grant (05441) and S. Nicholson the CSIR-UCT doctoral grant. The model data used are accessible on request to S. Nicholson.

References

Arrigo, K. R., G. L. van Dijken, and S. Bushinsky (2008), Primary production in the Southern Ocean, 1997–2006, *J. Geophys. Res.*, *113*, C08004, doi:10.1029/2007JC004551.

Aumont, O., and L. Bopp (2006), Globalizing results from ocean in situ iron fertilization studies, *Global Biogeochem. Cycles*, *20*, GB2017, doi:10.1029/2005GB002591.

Bowie, A. R., D. Lannuzel, T. A. Remenyi, T. Wagener, P. J. Lam, P. W. Boyd, C. Guieu, A. T. Townsend, and T. W. Trull (2009), Biogeochemical iron budgets of the Southern Ocean south of Australia: Decoupling of iron and nutrient cycles in the subantarctic zone by the summertime supply, *Global Biogeochem. Cycles*, *23*, GB4034, doi:10.1029/2009GB003500.

Bowie, A. R., et al. (2015), Iron budgets for three distinct biogeochemical sites around the Kerguelen Archipelago (Southern Ocean) during the natural fertilisation study, KEOPS-2, *Biogeosciences*, *12*(14), 4421–4445, doi:10.5194/bg-12-4421-2015.

Boyd, P. W. (2002), Environmental factors controlling phytoplankton processes in the Southern Ocean, *J. Phycol.*, *38*(2), 844–861.

Boyd, P. W., et al. (2005), FeCycle: Attempting an iron biogeochemical budget from a mesoscale SF, *Global Biogeochem. Cycles*, *19*, GB4S20, doi:10.1029/2005GB002494.

Brodeau, L., B. Barnier, A.-M. Treguier, T. Penduff, and S. Gulev (2010), An ERA40-based atmospheric forcing for global ocean circulation models, *Ocean Model.*, *31*(3-4), 88–104, doi:10.1016/j.ocemod.2009.10.005.

Carranza, M. M., and S. T. Gille (2015), Southern Ocean wind-driven entrainment enhances satellite chlorophyll-a through the summer, *J. Geophys. Res. Oceans*, *120*, 304–323, doi:10.1002/2014JC010203.
Cisewski, B., V. H. Strass, and H. Prandke (2005), Upper-ocean vertical mixing in the Antarctic Polar Front Zone, *Deep Sea Res., Part II*, *52*, 1087–1108.
Cisewski, B., V. H. Strass, M. Losch, and H. Prandke (2008), Mixed layer analysis of a mesoscale eddy in the Antarctic Polar Front Zone, *J. Geophys. Res.*, *113*, C05017, doi:10.1029/2007JC004372.
Daniault, N., and Y. Ménard (1985), Eddy kinetic energy distribution in the Southern Ocean from altimetry and FGGE drifting buoys, *J. Geophys. Res.*, *90*(C6), 11,877–11,889, doi:10.1029/JC090iC06p11877.
D'Asaro, E. A., P. Van Meurs, R. E. Davis, P. P. Niiler, C. C. Eriksen, and M. D. Levi (1993), Upper ocean inertial currents forced by a strong storm. I: Mixed layer. II: Propagation into the thermocline.
Dohan, K., and R. E. Davis (2011), Mixing in the transition layer during two storm events, *J. Phys. Oceanogr.*, *41*(1), 42–66, doi:10.1175/2010JPO4253.1.
Fauchereau, N., A. Tagliabue, L. Bopp, and P. M. S. Monteiro (2011), The response of phytoplankton biomass to transient mixing events in the Southern Ocean, *Geophys. Res. Lett.*, *38*, L17601, doi:10.1029/2011GL048498.
Forryan, A., A. C. N. Garabato, K. L. Polzin, and S. Waterman (2015), Rapid injection of near-inertial shear into the stratified upper ocean at an Antarctic Circumpolar Current front, *Geophys. Res. Lett.*, *41*, 1–11, doi:10.1002/(ISSN)1944-8007.
Frants, M., S. T. Gille, M. Hatta, W. T. Hiscock, M. Kahru, C. I. Measures, B. G. Mitchell, and M. Zhou (2013), Analysis of horizontal and vertical processes contributing to natural iron supply in the mixed layer in southern Drake Passage, *Deep Sea Res., Part II*, *90*(C), 68–76, doi:10.1016/j.dsr2.2012.06.001.
Hosoda, S., T. Ohira, K. Sato, and T. Suga (2011), Improved description of global mixed-layer depth using Argo profiling floats, *J. Oceanogr.*, *66*(6), 773–787, doi:10.1007/s10872-010-0063-3.
Jeandel, C., et al. (1998), KERFIX, a time-series station in the Southern Ocean: A presentation, *J. Mar. Syst.*, *17*(1–4), 555–569, doi:10.1016/S0924-7963(98)00064-5.
Jing, Z., L. Wu, L. Li, C. Liu, X. Liang, Z. Chen, D. Hu, and Q. Liu (2011), Turbulent diapycnal mixing in the subtropical northwestern Pacific: Spatial-seasonal variations and role of eddies, *J. Geophys. Res.*, *116*, C10028, doi:10.1029/2011JC007142.
Johnston, T. M. S., and D. L. Rudnick (2009), Observations of the transition layer, *J. Phys. Oceanogr.*, *39*(3), 780–797, doi:10.1175/2008JPO3824.1.
Klein, P., and G. Lapeyre (2004), Wind ringing of the ocean in presence of mesoscale eddies, *Geophys. Res. Lett.*, *31*, L15306, doi:10.1029/2004GL020274.
Lee, D. K., and P. P. Niiler (1998), The inertial chimney: The near inertial energy drainage from the ocean surface to the deep layer, *J. Geophys. Res.*, *103*(C4), 7579–7591, doi:10.1029/97JC03200.
Lévy, M. (2015), Exploration of the critical depth hypothesis with a simple NPZ model, *ICES J. Mar. Sci.*, *72*(6), 1916–1925, doi:10.1093/icesjms/fsv016.
Lévy, M., P. Klein, and M. Ben Jelloul (2009), New production stimulated by high-frequency winds in a turbulent mesoscale eddy field, *Geophys. Res. Lett.*, *36*, L16603, doi:10.1029/2009GL039490.
Llort, J., M. Lévy, J. B. Sallée, and A. Tagliabue (2015), Onset, intensification, and decline of phytoplankton blooms in the Southern Ocean, *ICES J. Mar. Sci.*, *72*(6), 1971–1984, doi:10.1093/icesjms/fsv053.
Meyer, A., B. M. Sloyan, K. L. Polzin, H. E. Phillips, and N. L. Bindoff (2015), Mixing variability in the Southern Ocean, *J. Phys. Oceanogr.*, *45*(4), 966–987, doi:10.1175/JPO-D-14-0110.1.
Morris, P. J., and M. A. Charette (2013), A synthesis of upper ocean carbon and dissolved iron budgets for Southern Ocean natural iron fertilisation studies, *Deep Sea Res., Part II*, 1–41, doi:10.1016/j.dsr2.2013.02.001.
Park, J., I. S. Oh, H. C. Kim, and S. Yoo (2010), Variability of SeaWiFs chlorophyll-a in the southwest Atlantic sector of the Southern Ocean: Strong topographic effects and weak seasonality, *Deep Sea Res., Part I*, *57*(4), 604–620.
Polton, J. A., J. A. Smith, J. A. MacKinnon, and A. E. Tejada Martínez (2008), Rapid generation of high-frequency internal waves beneath a wind and wave forced oceanic surface mixed layer, *Geophys. Res. Lett.*, *35*, L13602, doi:10.1029/2008GL033856.
Price, J. F., C. N. K. Mooers, and J. C. Van Leer (1978), Observation and simulation of storm-induced mixed-layer deepening, *J. Phys. Oceanogr.*, *8*(4), 582–599, doi:10.1175/1520-0485(1978)008<0582:OASOSI>2.0.CO;2.
Racault, M. F., C. Le Quéré, E. Buitenhuis, S. Sathyendranath, and T. Platt (2012), Phytoplankton phenology in the global ocean, *Ecol. Indic.*, *14*, 152–163, doi:10.1016/j.ecolind.2011.07.010.
Sun, O. M., S. R. Jayne, K. L. Polzin, B. A. Rahter, and L. C. S. Laurent (2013), Scaling turbulent dissipation in the transition layer, *J. Phys. Oceanogr.*, *43*(11), 2475–2489, doi:10.1175/JPO-D-13-057.1.
Swart, S., S. J. Thomalla, and P. M. S. Monteiro (2015), Journal of marine systems, *J. Mar. Syst.*, 1–13, doi:10.1016/j.jmarsys.2014.06.002.
Tagliabue, A., T. Mtshali, O. Aumont, A. R. Bowie, M. B. Klunder, A. N. Roychoudhury, and S. Swart (2012), A global compilation of dissolved iron measurements: Focus on distributions and processes in the Southern Ocean, *Biogeosciences*, *9*(6), 2333–2349, doi:10.5194/bg-9-2333-2012.
Tagliabue, A., J. B. Sallée, A. R. Bowie, M. Lévy, and S. Swart (2014), Surface-water iron supplies in the Southern Ocean sustained by deep winter mixing, *Nat. Geosci.*, *7*(4), 314–320, doi:10.1038/ngeo2101.
Thomalla, S. J., N. Fauchereau, S. Swart, and P. M. S. Monteiro (2011), Regional scale characteristics of the seasonal cycle of chlorophyll in the Southern Ocean, *Biogeosciences*, *8*(10), 2849–2866, doi:10.5194/bg-8-2849-2011.
Thomalla, S. J., M.-F. Racault, S. Swart, and P. M. S. Monteiro (2015), High-resolution view of the spring bloom initiation and net community production in the Subantarctic Southern Ocean using glider data, *ICES J. Mar. Sci.*, *72*(6), 1999–2020, doi:10.1093/icesjms/fsv105.
Wang, W., and R. X. Huang (2004), Wind energy input to the Ekman layer*, *J. Phys. Oceanogr.*, *34*, 1267–1275.
Yuan, X. (2004), High-wind-speed evaluation in the Southern Ocean, *J. Geophys. Res.*, *109*, 1–10, doi:10.1029/2003JD004179.
Yuan, X., J. Patoux, and C. Li (2009), Satellite-based midlatitude cyclone statistics over the Southern Ocean: 2. Tracks and surface fluxes, *J. Geophys. Res.*, *114*, D04106, doi:10.1029/2008JD010874.
Zhai, X., R. J. Greatbatch, and J. Zhao (2005), Enhanced vertical propagation of storm-induced near-inertial energy in an eddying ocean channel model, *Geophys. Res. Lett.*, *32*, L18602, doi:10.1029/2005GL023643.